ANNUAL REVIEWS

Annual Review of Materials Research

Grain Boundary Complexion Transitions

Patrick R. Cantwell,[1] Timofey Frolov,[2] Timothy J. Rupert,[3] Amanda R. Krause,[4] Christopher J. Marvel,[5] Gregory S. Rohrer,[6] Jeffrey M. Rickman,[5] and Martin P. Harmer[5]

[1]Rose-Hulman Institute of Technology, Terre Haute, Indiana 47803, USA; email: cantwep@rose-hulman.edu

[2]Lawrence Livermore National Laboratory, Livermore, California 94550, USA; email: frolov2@llnl.gov

[3]Department of Materials Science and Engineering, University of California, Irvine, California 92697, USA; email: trupert@uci.edu

[4]Department of Materials Science and Engineering, University of Florida, Gainesville, Florida 32611, USA; email: a.krause@ufl.edu

[5]Department of Materials Science and Engineering, Lehigh University, Bethlehem, Pennsylvania 18015, USA; email: cjm312@lehigh.edu, jmr6@lehigh.edu, mph2@lehigh.edu

[6]Department of Materials Science and Engineering, Carnegie Mellon University, Pittsburgh, Pennsylvania 15213, USA; email: rohrer@cmu.edu

Annu. Rev. Mater. Res. 2020. 50:465–92

First published as a Review in Advance on April 21, 2020

The *Annual Review of Materials Research* is online at matsci.annualreviews.org

https://doi.org/10.1146/annurev-matsci-081619-114055

Keywords

grain boundary, complexion, grain boundary phase, transmission electron microscopy, interface modeling, phase-like transitions

Abstract

Grain boundaries can undergo phase-like transitions, called complexion transitions, in which their structure, composition, and properties change discontinuously as temperature, bulk composition, and other parameters are varied. Grain boundary complexion transitions can lead to rapid changes in the macroscopic properties of polycrystalline metals and ceramics and are responsible for a variety of materials phenomena as diverse as activated sintering and liquid-metal embrittlement. The property changes caused by grain boundary complexion transitions can be beneficial or detrimental. Grain boundary complexion engineering exploits beneficial complexion transitions to improve the processing, properties, and performance of materials. Here, we review the thermodynamic fundamentals of grain boundary complexion transitions, highlight the strongest experimental and computational

evidence for these transitions, clarify a number of important misconceptions, discuss the advantages of grain boundary complexion engineering, and summarize existing research challenges.

1. INTRODUCTION

The term complexion refers to the thermodynamically stable state of an interface such as a grain boundary or phase boundary (1). In other words, a complexion is the material at an interface that is physically distinct from the abutting bulk phases, with an atomic structure and composition that are determined by thermodynamic parameters.[1] Using the term complexion for an interface is analogous to using the term phase for a bulk material because both complexions and phases are governed by the same thermodynamic principles. Grain boundaries can undergo phase-like transitions called grain boundary complexion transitions in which their structure and/or composition change abruptly as temperature or other thermodynamic parameters are varied, often causing discontinuous changes in grain boundary properties such as mobility, diffusivity, and cohesive strength (1, 3). Grain boundary complexion transitions can also cause rapid changes in the properties and performance of polycrystalline materials (4), playing a key role in many grain boundary–related phenomena, including activated sintering (5), liquid-metal embrittlement (6), and abnormal grain growth (7). These rapid changes in macroscopic behavior are remarkable because they typically occur independent of bulk phase transformations.

The history of grain boundary complexion transitions began in 1968 when E.W. Hart proposed that grain boundary transitions might be responsible for temper embrittlement and anomalous grain boundary segregation (8). Hart's prediction was made in analogy to surface phase transitions, which were well known at the time. Subsequent work by Hart (9), Cahn (10), and Tang et al. (2, 11) further elucidated the thermodynamics of grain boundary transitions. Seminal experimental work included the discovery of intergranular films in Si_3N_4 (12), the effect of complexion transitions on grain boundary mobility and abnormal grain growth in alumina (7), and the complexion transition that causes liquid-metal embrittlement in Ni-Bi (6). Recently, grain boundary complexion engineering has been proposed (13) as an approach to improve the properties and performance of polycrystalline engineering materials.

In this review, we introduce the thermodynamics of grain boundary complexion transitions, discuss seminal experimental and computational results, explain key features of successful computational approaches, and clarify common misconceptions. We also highlight studies that have simultaneously employed theory and experiment to elucidate grain boundary complexion behavior. This integration of theory and experiment is critical to meeting several of the future challenges we discuss at the end of the review.

2. GRAIN BOUNDARY COMPLEXION TRANSITION FUNDAMENTALS

In this section, we discuss the fundamentals of grain boundary complexion transitions by introducing a set of thermodynamic equations that model grain boundaries in a fluid-like manner. These simplified equations illustrate the key characteristics of grain boundary complexions and provide a good, albeit approximate, description of their behavior under hydrostatic stress. We then

[1] Prior to the term complexion being introduced in 2006 (2), many authors used phrases such as grain boundary phase or interfacial phase when referring to a grain boundary complexion or an interfacial complexion.

highlight an extension of these equations to include a nonhydrostatic mechanical stress state that is characteristic of grain boundaries.

2.1. Description of a Grain Boundary

The thermodynamically stable state of a grain boundary is defined by its structure and chemistry; therefore, traditional grain boundary parameters characterize a grain boundary complexion. There are both macroscopic and microscopic parameters that describe the grain boundary structure. The macroscopic grain boundary parameters include the three parameters describing the lattice misorientation between the grains and the two parameters describing the grain boundary plane orientation. The microscopic parameters include a vector describing the spatial displacement between the lattices. The parameters describing the grain boundary composition include the grain boundary excesses of segregating impurities and point defects. The amount of segregation and preferred atomic positions depend on the aforementioned structural parameters (14). Grain boundaries have additional characteristics such as boundary thickness, gradients in atomic structure and composition perpendicular to the boundary, and periodicity of atomic structure and composition parallel to the boundary. Taken together, these structural and compositional features of a grain boundary determine the free energy per unit area of the grain boundary, γ. This boundary free energy contributes to the total free energy of a polycrystal and is of central importance in the definition of a complexion transition.

2.2. Grain Boundary Equilibrium

The lowest free energy of a crystalline material would occur when all grain boundaries are eliminated, given the energy cost associated with broken bonds, etc., at a boundary. However, kinetic and geometric constraints typically prevent this from occurring, and a local equilibrium assumption is usually applied when analyzing a grain boundary (15, 16). When a grain boundary is in equilibrium with the bulk crystal, it adopts a well-defined structure and thermodynamically stable state characterized by excess quantities such as excess energy $[U]$, excess entropy $[S]$, excess volume $[V]$, the excess of component i at the interface[2] $[N_i]$, and γ. In this context, the square brackets denote an excess quantity per unit area,[3] the difference between that property in a system containing a grain boundary separating two bulk crystals and the corresponding quantity in a bulk crystal.

Interface thermodynamics was developed by Gibbs (17), who introduced these interfacial excess properties using the concept of the dividing surface. More recently, Cahn (18) proposed an alternative notation that offered a convenient mathematical way of expressing the excess quantities. We adopt Cahn's notation[4] (18) because it offers a simple expression for excess grain boundary volume, which, by definition, is zero in Gibbs's treatment.

The grain boundary free energy is an excess grand potential and can be written in Cahn's notation for a system containing C components as:

$$\gamma = [U]_{N_1} - T[S]_{N_1} + P[V]_{N_1} - \sum_{i=2}^{C} \mu_i [N_i]_{N_1}. \qquad 1.$$

[2]The terms grain boundary excess, grain boundary segregation, and grain boundary adsorption are often used interchangeably.
[3]Brackets are omitted from γ by convention.
[4]Here, $[Z]_{N_1}$ is $[Z/N_1]$ in Cahn's original notation.

In Equation 1, the subscript N_1 indicates that the system with the grain boundary and the bulk system contain the same number of atoms of the first component, N_1, i.e., the grain boundary excess $[N_1]_{N_1}$ is zero. The grain boundary excess of other components, such as $[N_2]_{N_1}$, may not be zero; they describe grain boundary segregation. The grain boundary free energy is a function of the temperature, pressure, and chemical potentials of the components as described by the Gibbs adsorption equation (17):

$$\mathrm{d}\gamma = -[S]_{N_1}\mathrm{d}T - [V]_{N_1}\mathrm{d}P - \sum_{i=2}^{C}[N_i]_{N_1}\mathrm{d}\mu_i. \qquad 2.$$

It is assumed that all excess quantities are continuous functions of the state variables T, P, and μ_i. The phase-like behavior of interfaces arises when multiple complexions can exist, each described by its own adsorption equation.

2.3. Definition of a Complexion Transition

Gibbs's analysis (17) can be considered the first rigorous thermodynamic treatment of complexion transitions. Although originally derived for fluid boundaries, it can be applied to other types of interfaces. Gibbs considered an interface that can exist in two different states, α and β, characterized by two different sets of excess quantities. He showed that in equilibrium the following relation holds:

$$\gamma^{\beta} - \gamma^{\alpha} \geq 0, \qquad 3.$$

where γ^{α} and γ^{β} are the excess free energies of two possible interface states, i.e., complexions. This relation dictates that in equilibrium the interface adopts the complexion with the lowest interfacial free energy, while the other complexion is metastable. If two different complexions have the same free energy, i.e., if $\gamma^{\alpha} = \gamma^{\beta}$, they can coexist in equilibrium. If a first-order transition were to occur at the exact equilibrium point, γ would remain constant while all other excess quantities would change discontinuously. To describe the grain boundary complexion coexistence space, consider the Gibbs adsorption equations for the two complexions:

$$\mathrm{d}\gamma^{\alpha} = -[S]^{\alpha}_{N_1}\mathrm{d}T - [V]^{\alpha}_{N_1}\mathrm{d}P - \sum_{i=2}^{C}[N_i]^{\alpha}_{N_1}\mathrm{d}\mu_i, \qquad 4.$$

$$\mathrm{d}\gamma^{\beta} = -[S]^{\beta}_{N_1}\mathrm{d}T - [V]^{\beta}_{N_1}\mathrm{d}P - \sum_{i=2}^{C}[N_i]^{\beta}_{N_1}\mathrm{d}\mu_i. \qquad 5.$$

Subtracting these equations and requiring that $\mathrm{d}\gamma^{\alpha} = \mathrm{d}\gamma^{\beta}$ along the coexistence line (19), we obtain

$$0 = -\Delta[S]_{N_1}\mathrm{d}T + \Delta[V]_{N_1}\mathrm{d}P - \sum_{i=2}^{C}\Delta[N_i]_{N_1}\mathrm{d}\mu_i. \qquad 6.$$

This equation describes how different thermodynamic variables, or degrees of freedom, can be varied while preserving equilibrium. It can be used to formulate Gibbs's phase rule for grain boundary complexions. Here, the number of degrees of freedom is $2 + C - 2$, where the first 2 represents the variables of T and P, C is the number of components, and the last 2 represents the two grain boundary complexions. In general, with m different grain boundary complexions, the number of degrees of freedom is $2 + C - m$ (19).

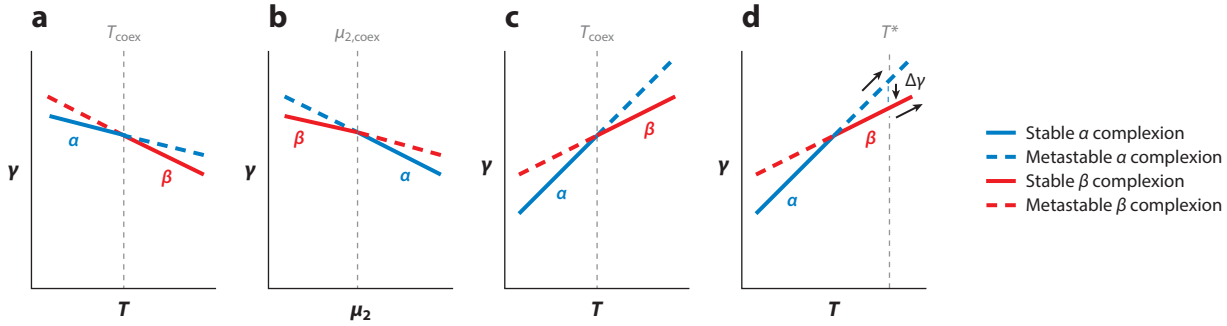

Figure 1

Complexion transitions between two complexions, α (*blue*) and β (*red*). Equilibrium coexistence may occur at T_{coex} (*a*) in a pure material at constant pressure and (*b*) in a binary material at constant pressure and constant temperature. In panels *c* and *d*, a thermally activated complexion transition in a hypothetical alloy occurs at constant pressure while temperature and chemical potential vary. In panel *c*, the complexion transition occurs under equilibrium conditions at T_{coex}, while in panel *d*, the transition is thermally activated, occurring at T^*.

A Clausius-Clapeyron equation for grain boundary complexions in a single-component system can also be derived (9, 19), with $[N]_N$ equal to zero, by applying Equation 6 to predict that the $P-T$ slope along the coexistence line is

$$\frac{\mathrm{d}P}{\mathrm{d}T_{coex}} = \frac{\Delta[S]_N}{\Delta[V]_N}. \qquad 7.$$

Equation 7 shows that at coexistence the single-component system has only one degree of freedom; if temperature is varied, pressure must also vary to maintain complexion equilibrium. If pressure is fixed, the two complexions can coexist at one temperature only. This case is shown in **Figure 1*a***, which illustrates a grain boundary complexion transition in a pure material, at fixed pressure. The free energies of the two complexions, α and β, cross at the equilibrium coexistence temperature, T_{coex}, where the two complexions coexist in equilibrium. Below T_{coex}, the low-temperature α complexion is stable, while above T_{coex}, the high-temperature β complexion becomes stable. Upon the complexion transition at T_{coex}, the slope of the free energy curve changes discontinuously. According to Equations 4 and 5, this discontinuous change is equal to the difference in the excess entropies, $\Delta[S]_N$, of the two complexions. It can also be shown that the slope discontinuity due to pressure-induced complexion transitions is given by the excess volume difference, $\Delta[V]_N$.

In addition to pressure and temperature, complexion transitions can be triggered by changes in chemical composition. **Figure 1*b*** schematically shows γ^α and γ^β of two grain boundary complexions in a binary system as functions of μ_2, at fixed temperature and pressure, which is related to the concentration of this component in the bulk crystals. According to the Gibbs adsorption equation, the slope of each curve is equal to the grain boundary segregation of the second component $[N_2]_{N_1}$. The stronger segregation to the α grain boundary complexion promotes a faster reduction in γ^α. The chemical potential value at which the free energies cross, $\mu_{2,coex}$, indicates the complexion transition, which is marked by a discontinuous change in the free energy slope given by the segregation difference $\Delta[N_2]_{N_1} = [N_2]^\beta_{N_1} - [N_2]^\alpha_{N_1}$. This thermodynamic analysis suggests that solutes stabilize the complexion with the higher amount of grain boundary segregation.

A complexion transition in a hypothetical alloy system is shown in **Figure 1*c*** at constant pressure, while temperature and chemical potentials vary. Note that γ has the opposite temperature dependence when compared with the pure material in **Figure 1*a***. In the pure material, γ decreases

with temperature because of entropic effects. However, this is a relatively small effect of less than 0.1 J/m^2 over a 100°C temperature interval (20). In doped or alloyed materials, there can be a more significant effect that can increase γ with temperature. In the most common case, illustrated in **Figure 1*c***, the solid solubility increases with temperature, enabling the solute to desegregate from the grain boundary and move to the bulk matrix. This desegregation lowers the grain boundary excess of impurities or alloying elements, which, in most cases, leads to increased grain boundary energy with increasing temperature, as in **Figure 1*c***. If superheating is required to nucleate the complexion transition, there may be a discontinuous change in grain boundary free energy, $\Delta\gamma$, as illustrated in **Figure 1*d***. Such a discontinuity may also occur in pure materials and, in general, in situations where equilibrium is not maintained during the transition. We emphasize that the complexion behavior in alloys discussed here is only one possible case; other cases exist, some with opposite temperature dependencies for γ and segregation.

The preceding discussion of grain boundary complexion transitions is based on the simplified, hydrostatic, fluid-like treatment of grain boundaries that neglects additional thermodynamic degrees of freedom available to solid interfaces. These equations can be extended to account for these additional degrees of freedom. For example, Frolov & Mishin (21) developed thermodynamic equations for solid interfaces in a multicomponent system that include the effects of a nonhydrostatic mechanical stress state. For grain boundaries, they developed the following adsorption equation that includes the effects of interface stress and shear stress parallel to the boundary plane:

$$\mathrm{d}\gamma = -[S]_N \mathrm{d}T - \sum_{k=2}^{C} [N_k]_N \mathrm{d}M_{k1} - \sum_{l=1}^{L} [n_l]_N \mathrm{d}\mu_l - \sum_{i=1,2,3} [V\overline{F}_{i3}/\overline{F}_{33}]_N \mathrm{d}\sigma_{3i} + \sum_{i,j=1,2} (\tau_{ij}^N - \delta_{ij}\gamma)\mathrm{d}e_{ij}, \quad 8.$$

where N is the total number of substitutional atoms, N_k is the number of atoms of substitutional component k, M_{k1} are diffusion potentials, n_l and μ_l are the number of atoms and chemical potentials of the interstitial components, $[V]_N$ is the excess volume, $[V\overline{F}_{13}/\overline{F}_{33}]_N$ and $[V\overline{F}_{23}/\overline{F}_{33}]_N$ are the excess shears, and τ_{ij}^N is the grain boundary stress tensor.

Equation 8 can be written for two grain boundary complexions, in analogy to Equations 4 and 5, to produce expressions for $\mathrm{d}\gamma^\alpha$ and $\mathrm{d}\gamma^\beta$. Subtracting these adsorption equations for two complexions and requiring that $\mathrm{d}\gamma^\alpha = \mathrm{d}\gamma^\beta$, the following equation is obtained:

$$0 = -\Delta[S]_N \mathrm{d}T - \sum_{k=2}^{C} \Delta[N_k]_N \mathrm{d}M_{k1} - \sum_{l=1}^{L} \Delta[n_l]_N \mathrm{d}\mu_l - \sum_{i=1,2,3} \Delta[V\overline{F}_{i3}/\overline{F}_{33}]_N \mathrm{d}\sigma_{3i} + \sum_{i,j=1,2} \Delta(\tau_{ij}^N - \delta_{ij}\gamma)\mathrm{d}e_{ij}. \quad 9.$$

Equation 9 is analogous to Equation 6 in that it describes equilibrium between two grain boundary complexions. We note that Equations 8 and 9 include the simplifying assumption that the nonhydrostatic mechanical stress is symmetric, which implies that the two grains adjacent to the grain boundary experience identical thermodynamic conditions and are therefore of identical composition. In the more general case in which the stress states in the two grains are different, they may exist in equilibrium yet have different compositions; therefore, the interface between them should be treated as a phase boundary rather than a grain boundary. Frolov & Mishin (21) also developed equations to describe a phase boundary that could be applied to this more general case.

2.4. Clarifications

In the recent literature, some misconceptions about complexion transitions exist that are worth clarifying. First, we emphasize that the field of grain boundary complexion transitions is a direct extension of traditional grain boundary knowledge and thermodynamics, rather than an

alternate theory of grain boundary behavior. One reason for this misunderstanding may have been the inconsistent usage of nomenclature over the years to describe complexion transitions. For example, grain boundary structural transitions, faceting transitions, and roughening transitions are all examples of grain boundary complexion transitions. The term grain boundary complexion transition is therefore particularly useful as a unifying concept that encompasses all thermodynamically induced grain boundary transformations involving atomic structure and/or composition.

We note that the phrase grain boundary phase is sometimes used instead of grain boundary complexion (e.g., 8–10, 22), in particular in work published before the term complexion was introduced in 2006 (2). The term complexion is preferred because interfaces do not meet the definition of a phase, since they are inhomogeneous and stable only when in contact with abutting bulk phases (1). Moreover, the term complexion unambiguously differentiates interfaces, such as grain boundaries, from bulk phases that may reside at an interface, such as bulk wetting phases and second-phase precipitates.

It has been noted that at a certain temperature or bulk composition, a grain boundary complexion appears or is formed. In fact, all well-defined states of the grain boundary are complexions, so the appearance of a complexion is typically the observation of a previously unknown complexion or of a complexion transition. In other cases, authors have dismissed complexion transitions as a possibility in materials with no added impurities. However, complexion transitions can also occur at clean grain boundaries in pure materials; examples of such transitions include faceting and roughening transitions induced by changes in temperature.

The question sometimes arises as to whether a grain boundary must be at global equilibrium to be a complexion; it need not be. Grain boundaries at local equilibrium are still complexions, and grain boundaries away from equilibrium may be called metastable complexions (2), by analogy with metastable bulk phases.

The way in which complexions are categorized is often a point of confusion. The six Dillon-Harmer categories of complexions, i.e., Types I–VI (7), have become popular for categorizing complexions. However, these six types were originally proposed for the specific case of grain growth in Al_2O_3, with numerical rankings based on grain boundary mobility. Instead of numbers I through VI, we recommend using descriptive terms to categorize complexions related to the important phenomenon that is active; common examples include thickness, solute content, and/or structure.

For example, a grain boundary in a pure material with no discernable solute adsorption could be referred to as a clean grain boundary complexion. A clean grain boundary complexion is shown in **Figure 2*a*** at a symmetric tilt boundary in copper. If bismuth is added to the copper, it segregates to this boundary in such a way that the majority of adsorbed solute atoms exist in a single atomic layer, as shown in **Figure 2*b***. This complexion, on the basis of visual inspection, may be categorized as a monolayer[5] grain boundary complexion according to the nomenclature suggested in a previous review (1). However, it does not necessarily follow that a clean-to-monolayer complexion transition has occurred due to the Bi segregation when comparing **Figure 2*a*,*b***. To determine if a complexion transition occurred, additional evidence would be needed, such as determining whether there is a discontinuity in the grain boundary energy (as described in the previous section) or, perhaps more practically, whether there is a discontinuous jump in Bi grain boundary segregation at a particular temperature or bulk composition. For the sake of discussion, let us assume that the clean-to-monolayer complexion did indeed occur, while noting that we lack sufficient evidence for this assumption. Since the structural units in the grain boundary are identical

[5] We note that terms such as monolayer are useful as a shorthand way of referring to a grain boundary complexion based on some of its observable features but do not completely describe its structure or all of its relevant features and properties.

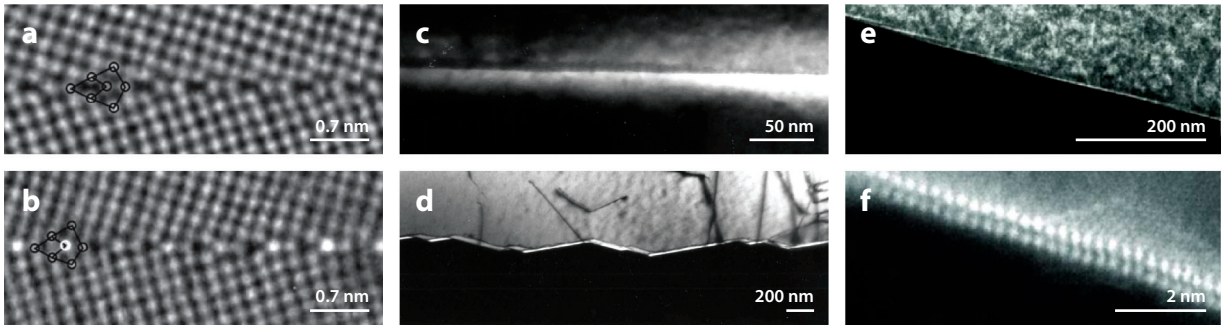

Figure 2

Grain boundary complexions in the Cu-Bi system. (*a*,*b*) A symmetric tilt boundary in copper (*a*) in a bicrystal with no Bi and, hence, no Bi adsorption at the grain boundary and (*b*) in a doped bicrystal containing 25 atomic ppm Bi and annealed at 700°C, exhibiting a monolayer of Bi adsorption at the grain boundary. (*c*) A grain boundary in a copper bicrystal containing 14 atomic ppm Bi and annealed at 600°C. (*d*) A grain boundary in a copper bicrystal containing 64 atomic ppm Bi and annealed at 800°C, exhibiting faceting. (*e*,*f*) Grain boundaries in polycrystalline copper that were annealed in contact with Bi-Cu liquids, exhibiting (*e*) faceting and (*f*) a bilayer of Bi adsorption. Panels *a* and *b* adapted with permission from Reference 137, panels *c* and *d* adapted with permission from Reference 23, and panels *e* and *f* adapted with permission from Reference 24.

in both complexions in **Figure 2*a*,*b***, and since no change in grain boundary plane orientation occurred, this conjectural situation would be an example of a congruent complexion transition. Sigle et al. (23) demonstrated that bismuth segregation to copper grain boundaries can indeed produce noncongruent complexion transitions in which a flat grain boundary undergoes a faceting complexion transition that produces two new grain boundary plane orientations. This noncongruent faceting complexion transition is illustrated in **Figure 2*c*,*d***, which show a nonfaceted grain boundary in Bi-doped Cu and a faceted grain boundary induced by higher temperature and higher Bi content, respectively. More recent experiments by Kundu et al. (24) have shown that a Bi-induced faceting complexion transition can also be accompanied by a complexion transition to a bilayer complexion, as shown in the low-magnification view of a faceted grain boundary in **Figure 2*e*** and the high-magnification view of a grain boundary in **Figure 2*f***, which exhibits a bilayer of Bi segregation.

The above examples in the Cu-Bi system illustrate that the term complexion transition may refer to an adsorption transition (e.g., clean-to-monolayer) or to a structural transition (e.g., noncongruent or faceting). If both types of complexion transitions are of interest for the phenomena under study, then an effort should be made to use complexion terminology that emphasizes the features of both.

Due to the large number of grain boundary complexions and transitions, a full exposition on recommended terminology is beyond the scope of this review. The interested reader is referred to a previous review article (1) that includes an extensive discussion of recommended terminology, explains how it relates to inconsistent terminology used over the years by various authors working in the field, and provides definitions for each term.

3. RECOGNIZING COMPLEXION TRANSITIONS

3.1. Evidence of Complexion Transitions

During a grain boundary complexion transition, there is a discontinuous change in the characteristics and properties of the boundary. Broadly speaking, two categories of evidence exist that indicate a complexion transition has occurred: direct and indirect evidence. We define direct evidence

as discontinuous changes in the structure, composition, and equilibrium properties of the grain boundary, e.g., excess entropy, volume, and the slope of the grain boundary free energy. We call this evidence direct because it directly relates to the thermodynamic definition of a complexion transition. Indirect evidence includes discontinuous changes in other properties of the grain boundary, such as kinetic, mechanical, thermal, and electrical properties. Direct and indirect evidence can be obtained both experimentally and computationally. When complexion transitions occur in a polycrystalline material, not all grain boundaries will necessarily transition simultaneously. Therefore, unusually rapid changes (rather than discontinuous changes) in grain boundary–related properties in polycrystals may be considered evidence of complexion transitions as well due to the averaging of properties between boundaries that have transitioned and those that have not.

3.2. Review of Direct Evidence of Complexion Transitions

Excess grain boundary energy characterizes a boundary thermodynamically and is therefore useful for identifying complexion transitions, but it is difficult to access directly via experimentation. Most measurements of boundary energy are therefore inferred from two types of experiments, namely, (*a*) grain boundary thermal grooving and (*b*) calorimetry data. When a grain boundary meets a surface, it can form an equilibrium groove whose geometry is determined by the balance of interfacial energies between the grain boundary and free surfaces (25). By measuring the groove with atomic force microscopy, the ratio between grain boundary energy and surface energy, i.e., the relative grain boundary energy, may be calculated. Several assumptions exist, giving limited meaning to a single measurement from one grain boundary groove (e.g., see 20). Nevertheless, if many measurements are made on many grooves, the average relative boundary energy and the width of the energy distribution are useful quantities (26). Dillon et al. (27) made such measurements in undoped and doped Al_2O_3, finding that complexion transitions can reduce the grain boundary energy up to 45%. Bojarski et al. (28) performed a similar study in yttria doped with Ca, finding that complexion transitions can increase both the anisotropy of the grain boundary energy and the grain boundary character distribution. These results demonstrate that grain boundary complexion transitions can have a wide-ranging impact on the network of grain boundaries throughout a polycrystalline material.

Differential scanning calorimetry can provide another quantity related to grain boundary energy by tracking the heat released during a grain growth experiment (29). Muche et al. (30) used this technique to obtain the grain boundary energy during the coarsening of nanocrystalline $MgAl_2O_4$. They found that boundary energy was a function of grain size, which was explained by a size-dependent cation site inversion effect. Dey et al. (31) used calorimetry to probe how boundary energy in nanocrystalline yttrium-stabilized zirconia was affected by La segregation, finding a reduction in the boundary energy and, therefore, the driving force for grain growth.

Atomistic modeling using molecular dynamics (MD) or Monte Carlo (MC) simulation can provide evidence of complexion transitions by predicting grain boundary energy changes and other relevant characteristics. A number of algorithms and databases exist for building grain boundary models for atomistic simulations (e.g., 32–34). Such models can then be exposed to thermodynamic conditions of interest. For example, Olmsted et al. (35) demonstrated a dislocation pairing complexion transition at high temperature in a low-angle Fe grain boundary. Frolov et al. (36) reported a reversible first-order complexion transition in two $\Sigma 5$ grain boundaries in pure Cu as temperature was varied during MD simulations. These authors implemented an important new feature in their atomic-scale simulations by adding a free surface to one or two sides of their simulation cell to allow for density variations along the grain boundary plane enabled by diffusion to these surfaces.

Later work by Frolov and coworkers (37) showed that a complexion transition between two kite structures may occur as a function of alloy composition in Cu-Ag, with the grain boundary free energy calculated by combining atomistic modeling with thermodynamic theory. Brown & Mishin (38) used MD models to probe the faceting of asymmetric tilt grain boundaries in Cu, finding an interesting subset of complexion transitions where the boundary area increases yet the overall interfacial energy decreases due to faceting. Rickman et al. (39) compiled complexion diagrams for a binary alloy using semigrand MC simulations in conjunction with modern histogram reweighting techniques. In addition to structurally ordered boundaries, MC simulations have been used to study the grain boundary energetics of a premelting transition to an amorphous intergranular film in Cu-Ag (40).

Discontinuous changes in the structure or chemical composition of grain boundaries are also direct evidence of complexion transitions. Experimental efforts to characterize grain boundary structure and chemistry often use transmission electron microscopy (TEM), scanning transmission electron microscopy (STEM), or atom probe tomography (APT). For example, Merkle & Smith (41) observed two coexisting grain boundary structures at a $\Sigma 5(310)$ boundary in NiO. Sickafus & Sass (42) found grain boundary structural transitions induced by solute segregation in a low-angle twist boundary in Fe-Au. Dillon et al. (7) used high-angle annular dark-field (HAADF)-STEM to uncover six grain boundary complexion types in Al_2O_3 that were differentiated by mobility. Khalajhedayati & Rupert (43) explored the critical temperature to form amorphous intergranular films in nanocrystalline Cu-Zr alloys, finding such films at and above 850°C, consistent with prior thermodynamic predictions (44). Two STEM investigations by Ma et al. revealed coexisting complexions with differing thicknesses and adsorbate levels along a single grain boundary, in both Si-Au (45) and CuO-doped TiO_2 (46), which were frozen partway through a first-order complexion transition during cooling. A combined TEM/APT technique has recently been used to identify phenomena as varied as segregation-induced faceting transitions (47), spinodal-like fluctuations in a grain boundary as a precursor to an equilibrium phase transformation (48), and grain boundary segregation that varied depending on the grain boundary character (49).

Computational models have also revealed grain boundary complexion transitions evidenced by discontinuous changes in structure and composition. For example, Williams & Mishin (50) used MC simulations to uncover premelting transitions at a $\Sigma 5(210)$ grain boundary in Cu-Ag. Pan & Rupert (51) employed a hybrid MC/MD method, finding that a segregation-induced transition to a disordered grain boundary complexion structure depended on the relative solute excess at the boundary. Simulations by Frolov and coworkers (37, 47) identified a dramatic jump in dopant excess at the grain boundary during a complexion transition that also altered the boundary structure. O'Brien et al. (52) reported a complexion transition between low and high solute content interfacial regions in Pt-Au, providing a striking example of how an interface can undergo phase-like separation that is similar to classical examples in the bulk. The fine resolution of atomic-scale modeling means that subtle transitions in structure can be studied. In particular, Yang et al. (53) found a transformation that breaks the mirror symmetry of a $\Sigma 5(210)$ grain boundary in Mo-Ni, while Pan & Rupert (54) uncovered spatial variations in short-range structural order within nanoscale amorphous intergranular films. Using evolutionary grain boundary structure search and MD simulations, Zhu et al. (55) and Frolov et al. (56) demonstrated new complexion transitions in elemental face-centered cubic (fcc) and body-centered cubic (bcc) metals within a wide range of misorientations and boundary types, including tilt and twist boundaries. Finally, Tewari et al. (57) identified Cl segregation in transparent polycrystalline alumina with STEM energy dispersive spectroscopy and employed atomistic simulations that demonstrated a solute-induced, first-order grain boundary complexion transition caused by the Cl impurities.

3.3. Review of Indirect Evidence of Complexion Transitions

Since transport across or along the grain boundary is intimately tied to grain boundary structure and composition, discontinuous changes in grain boundary diffusivity and mobility can serve as indirect evidence of a complexion transition. In fact, most of the complexion transitions that have been identified experimentally were found via anomalous changes in grain growth behavior. For example, Molodov et al. (58) identified a large increase in grain boundary mobility in aluminum with very small additions of Ga, which they attributed to a prewetting complexion transition. As noted above, Dillon & Harmer (59) and Dillon et al. (7) observed six different grain boundary complexions with different mobilities in Al_2O_3, and they correlated these complexions with fast- and slow-growing grains during abnormal grain growth.

With regards to diffusivity, Divinski et al. (60) measured a discontinuous jump greater than two orders of magnitude in grain boundary diffusivity in Cu-Bi, which they attributed to a premelting complexion transition. In another study, a deviation from linear Arrhenius dependence of Ag diffusivity on temperature was observed in a $\Sigma 5(310)[001]$ grain boundary in Cu, which was attributed to a structural grain boundary transition (61). This transition was subsequently found by atomistic simulations (62). Prokoshkina et al. (63) studied grain boundary diffusion of Fe in Cu-Fe alloys and found a three orders of magnitude increase in the triple product of grain boundary diffusion (product of the diffusion coefficient, diffusion width, and segregation factor) for Fe at high dopant concentrations. Diffusivity enhancements due to complexion transitions have also been linked to the long-known phenomenon of activated sintering, with a complexion transition from ordered grain boundaries to amorphous intergranular films being frequently cited as the mechanism. For example, the addition of CuO to TiO_2 drives a transition to disordered boundary films with nanoscale thicknesses and allows for sintering of powders a full 300°C below the eutectic temperature (64).

Mechanical property changes also serve as indirect evidence of complexion transitions. For example, Sigle et al. (65) showed that Ga embrittlement of Al is connected to the formation of layered Ga segregation at the grain boundaries. Similarly, Luo et al. (6) demonstrated that weakly bonded Bi atoms in a bilayer complexion were responsible for liquid-metal embrittlement in Ni-Bi. Rupert and coworkers demonstrated that amorphous intergranular films both toughen (66, 67) and strengthen (43, 68) nanocrystalline metals. Similarly, Madhav Reddy et al. (69) found that amorphous complexions improve the compressive strength, plasticity, and toughness of nanocrystalline B_4C. A direct method for measuring the toughening effect of complexions was introduced by Cui et al. (70), although they found no change in the boundary fracture toughness of Eu-doped $MgAl_2O_4$. A similar technique was used by Feng et al. (71) to show that a submonolayer complexion could have a higher fracture toughness than a clean grain boundary.

4. COMPLEXION TRANSITIONS IN POLYCRYSTALLINE MATERIALS

In this section, we critically review evidence that suggests a new conceptual framework that can be used to explain how grain boundary complexion transitions may lead to heterogeneous microstructures in polycrystalline materials. While all grain boundaries share the characteristic of separating crystals of different orientations, they have a wide range of different energies and structures (72). The role of boundary structure and energy in dictating boundary thermodynamics was recognized in early theoretical work on complexions, where it was found that higher energy grain boundaries are more susceptible to transitioning at a given temperature than lower energy boundaries (2). This result was confirmed by experiments (73) in which polycrystalline Y-doped Al_2O_3 was sandwiched between single crystals of Al_2O_3 terminated by different crystallographic planes

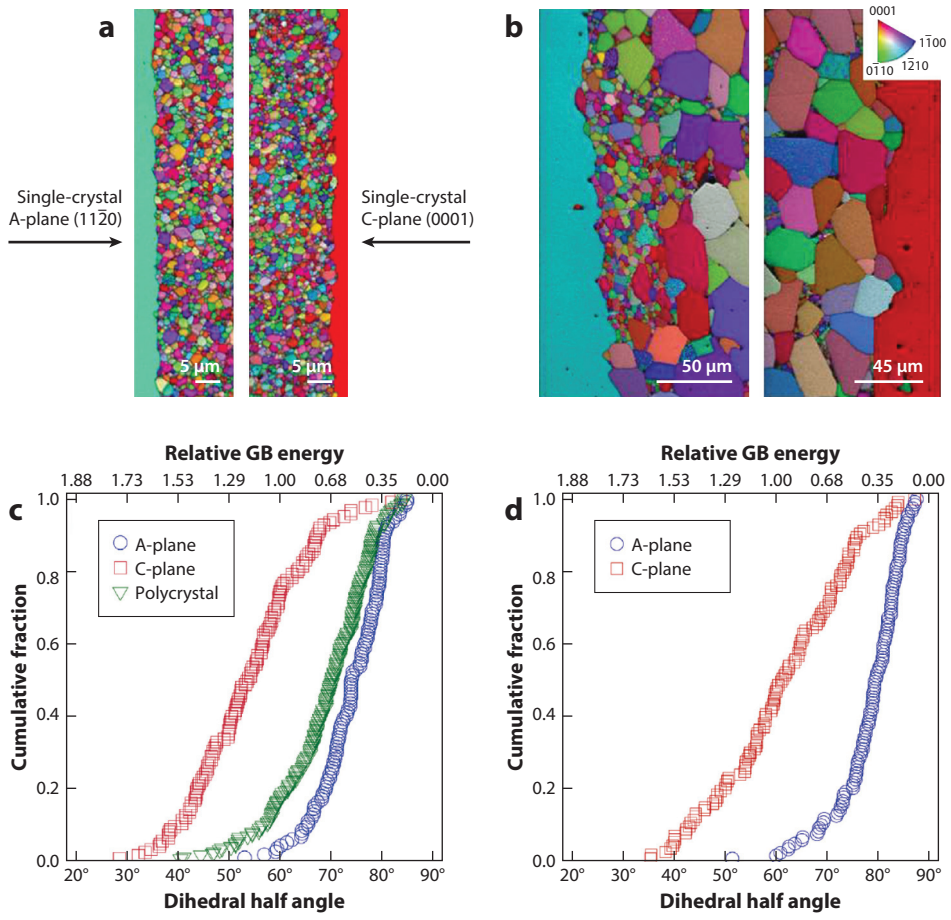

Figure 3

Polycrystalline Y-doped Al_2O_3 sandwiched between two single crystals of Al_2O_3 with different orientations. Electron backscatter diffraction orientation maps near the A-plane and C-plane single-crystal interfaces illustrate the grain size (*a*) before annealing and (*b*) after annealing for 8 h at 1,500°C. Relative grain boundary (GB) energy distributions near the single-crystal interfaces (*c*) before annealing and (*d*) after annealing reveal that GBs along the C-plane had a higher average energy than those along the A-plane and that the average energy of these boundaries decreased during annealing. Figure adapted with permission from Reference 73.

and then annealed. During annealing, higher energy grain boundaries preferentially underwent complexion transitions to higher mobility complexions, as illustrated in **Figure 3**. The electron backscatter diffraction maps in **Figure 3*a*** show that the grain size near both single crystals is similar before annealing. In contrast, **Figure 3*b*** shows that after annealing the grains in contact with the C-plane single-crystal interface are much larger due to transitions to higher mobility grain boundary complexions. These complexion transitions occurred preferentially along the C-plane because of the higher grain boundary energies along this interface, as illustrated by the relative grain boundary energy distributions in **Figures 2*d*** and **3*c***. This experiment demonstrates that, during isothermal annealing, some subset of high-energy boundaries can transform to a new complexion while others remain stable. Therefore, understanding variations in grain boundary energy is the key to understanding this heterogeneous behavior.

In pure materials, grain boundary energies vary with geometry, temperature, and pressure. While little is known about variations with pressure, it is known that the grain boundary energy of pure materials decreases with temperature, while that of impure materials sometimes increases with temperature, as illustrated in **Figure 1**. At fixed temperature, the source of the heterogeneity of the grain boundary energies is grain boundary geometry. Experimental measurements have shown that grain boundary energies vary by at least a factor of three (74), with calculations suggesting that the highest energy boundaries can have energies that are 4 (75) to 13 (76) times higher than those of the lowest energy boundaries. This variation is due to the presence of a small population of boundaries with particularly low energy. For example, the twin boundary in an fcc metal has one-tenth the average boundary energy, while most grain boundaries have energies in a range that differs from the average energy by about 40%. However, in materials that evolve by normal grain growth, lower energy grain boundaries dominate the population, so a complete range of boundary energies is expected in most microstructures (77). Therefore, at fixed temperature, if grain boundaries above a certain energy threshold transform and those below do not, the heterogeneity of grain boundary properties increases.

Impurities and alloying elements can significantly alter boundary energetics. As discussed in Section 4, the sign of the grain boundary energy change with temperature in an impure material can be the opposite of that in a pure material. This occurs if the solid solubility increases with temperature and the grain boundary energy is inversely related to the grain boundary excess. There is also an interesting influence of grain size on the grain boundary excess, the grain boundary energy, and complexion transitions. To understand this, we introduce the concept of extrinsic solubility (78). Within any single-phase polycrystal, impurities can be partitioned to two locations: the matrix (dissolved within the grains) or the grain boundaries. The amount of solute partitioned to the matrix is exactly accounted for by the bulk or intrinsic solubility, which does not change with grain size. However, the total amount of solute (rather than the concentration) segregated to the grain boundary depends on the total grain boundary area. In a single crystal, this amount is zero because there is no grain boundary area. In a polycrystal with grain boundary area A and grain boundary excess per area $[N_2]_{N_1}$, the amount of solute partitioned to the grain boundaries is $A[N_2]_{N_1}$. Therefore, the excess solute concentration, C_{ex}, in a polycrystal of volume V and atomic concentration ρ (of the matrix atoms) is $C_{ex} = (A[N_2]_{N_1})/(\rho V)$. For cube-shaped grains with surface area $6D^2$ and volume D^3, $C_{ex} = (3[N_2]_{N_1})/(\rho D)$. The excess solute increases as the grain size decreases. In a specimen with a sufficiently large grain size and intrinsic solubility, this excess is negligible. However, if we assume the intrinsic solubility is very small, the atomic concentration of the matrix (solvent) is 45 atoms/nm^3, and the boundary excess is 7.5 atoms/nm^2, then at a grain size of $D = 1$ μm, the extrinsic concentration is 500 ppm. If the grain size decreases into the nanometer range, the excess solute increases significantly.

This introduces interesting possibilities for how grain boundary composition and energy may change with grain size. In the hypothetical example above, if the average grain size increases and the grain boundary area decreases, the grain boundary excess will increase. As it increases, the grain boundary energy will decrease, illustrating the apparent influence of grain size on grain boundary energy. Ultimately, an upper limit of grain boundary excess must be reached. Further increases in grain size and decreases in grain boundary area must then be accommodated by a grain boundary complexion transition or the precipitation of a new phase (79).

Therefore, grain boundary energy can be influenced by temperature in several ways depending on the sample composition and grain size and because there is a wide range of grain boundary energies. We summarize key results from some relevant studies on this issue and then discuss their implications. The effects of temperature and complexion transitions on the grain boundary energy in Y-doped alumina were explored by Kelly et al. (78). First, it was found that relative

grain boundary energy with no added impurities decreased slightly with increasing temperature, as expected. For 100 and 500 ppm Y-doped alumina, the grain boundary energy increased with temperature, again as expected for an impure material. However, abrupt decreases in grain boundary energy occurred between 1,450°C and 1,550°C, which are ascribed to the phenomenon illustrated in **Figure 1*d*** in which superheating is needed for the transformation. These decreases occurred over a range of 100°C because of the anisotropy of the grain boundary energy, with higher (lower) energy boundaries transforming at lower (higher) temperatures.

The localized nature of these transitions to specific grain boundaries and the neighborhood around them was illustrated in a study on $SrTiO_3$, in which a transition in mobilities leads to abnormal grain growth (80) and, in the temperature range of this transition, there is a combination of boundaries moving relatively fast and slow. This situation was ascribed to a complexion transition, although without atomic-scale structural evidence (81). Relative grain boundary energy measurements at triple junctions revealed that the fast boundaries had consistently higher energies than the slow boundaries at the same temperature (82). This suggests the coexistence of grain boundaries in two different complexions with two distinct distributions of energies and mobilities.

The results highlighted here lead to a new conceptual understanding by suggesting that both the anisotropy of the grain boundary energy and the need to activate the transition lead to heterogeneous polycrystalline microstructures. One outstanding question is, how do enough grain boundaries surrounding a single grain transform to create a bimodal microstructure of large grains with fast-moving boundaries and slow grains with slow-moving boundaries? If a complexion transition strictly depended on grain boundary energy with no required activation, a random distribution of transforming boundaries would be expected. This proposition was recently tested by simulation, and abnormal grains were not observed when boundaries distributed at random positions transformed to a high mobility complexion, contrary to experimental observations (83). Fast-growing abnormal grains were sustainable only when complexion transformations happened in a spatially correlated way, where a boundary is more likely to transform if it abuts a transformed boundary. This result suggests that an activation barrier exists and that boundaries in contact with a transformed boundary can more easily overcome this barrier.

5. EXPERIMENTAL CHARACTERIZATION OF COMPLEXIONS

Experimental investigations of complexions and their transitions require techniques that can determine grain boundary structure, chemistry, and composition on both macroscopic and atomic scales. **Table 1** summarizes common experimental approaches. Two heavily utilized methods for atomic-scale characterization are TEM and STEM, collectively referred to as S/TEM. S/TEM provides the unique ability to determine grain boundary structure and composition via atomic-resolution imaging and spectroscopy. Quantitative complexion structural metrics (e.g., interface step sizes, terminal plane, boundary thickness) and compositional metrics, which can potentially be used as inputs to computational simulations, are also experimentally accessible using S/TEM.

While S/TEM allows precise measurements of atomic column positions, it has some limitations for the study of complexion transitions. First, the images are a two-dimensional projection of a three-dimensional material, which causes a loss of information. Sometimes this loss can be overcome, as when Yu et al. (84) supplemented STEM results with density functional theory (DFT) to demonstrate the existence of segregation superstructures at general grain boundaries in Ni-Bi. One result from this study is shown in **Figure 4**. The HAADF-STEM image of the grain boundary reveals periodic Bi segregation, but since it is a two-dimensional projected image, it lacks information about atomic periodicity in the third dimension, i.e., the electron beam

Table 1 Summary of common experimental characterization techniques to determine complexion structure, composition, and chemical bonding configurations

Instrumentation	Imaging or spectroscopy modality	Advantages	Disadvantages
Grain boundary structure			
STEM	HAADF imaging	Directly interpretable atomic positions based on atomic number contrast; can image submonolayers, monolayers, bilayers, etc. (e.g., see 7)	Prone to grain boundary inclination; inherently a 2D method to image a 3D structure (84)
	ABF imaging	Light element detection	Requires very thin specimen for best results (typically $\ll$50 nm)
TEM	HRTEM via phase contrast imaging	Periodic structure (optimal imaging mode for submonolayer and nanolayer complexions)	Requires specimen thickness and defocus information to reconstruct image into directly interpretable results
SEM	EBSD	Determines macroscopic misorientation between grains; 3D EBSD via serial sectioning with an FIB can determine GBCD and GBED (74)	Requires thousands of grain boundary segments to generate accurate grain boundary energy and character distributions; 3D EBSD is destructive and requires FIB capability in addition to SEM
3D XRD	NA	Nondestructively determines 3D grain boundary misorientations of polycrystals	Generally requires synchrotron light sources; tabletop instrumentation is improving
Grain boundary chemistry and composition			
STEM	EDS (a.k.a. XEDS)	Can analyze the full range of elements with proper standard-based quantification; can determine excess planar coverages (i.e., atoms/nm^2) (85–87); elemental mapping to show 2D chemical distributions (88)	Poor signal (relative to EELS); larger X-ray interaction volume reduces the spatial resolution; poor at light elements; cannot identify bonding states; poor energy resolution (problematic for overlapping signals from different elements)
	EELS	Directly determines bonding configurations of elemental constituents on the grain boundaries (89)	Experimental error when determining absolute grain boundary composition due to background subtraction difficulties
TEM	EFTEM imaging	Efficient qualitative results based on EELS	High error for composition quantification
APT	NA	3D representation of grain boundary chemistry/composition (90); light element detection (91); molecular ion detection (92)	Does not provide atomic position at a sufficiently high precision to determine crystallographic information
Nano-SIMS	NA	Light element detection; isotopic sensitivity	Requires accurate standards for proper quantification

Abbreviations: ABF, annular bright-field; APT, atom probe tomography; EBSD, electron backscatter diffraction; EDS, energy dispersive spectroscopy; EELS, electron energy loss spectroscopy; EFTEM, energy-filtered transmission electron microscopy; FIB, focused ion beam; GBCD, grain boundary character distribution; GBED, grain boundary energy distribution; HAADF, high-angle annular dark-field; HRTEM, high-resolution transmission electron microscopy; NA, not applicable; Nano-SIMS, nano-secondary ion mass spectroscopy; SEM, scanning electron microscopy; STEM, scanning transmission electron microscopy; TEM, transmission electron microscopy; XEDS, X-ray energy dispersive spectroscopy; XRD, X-ray diffraction.

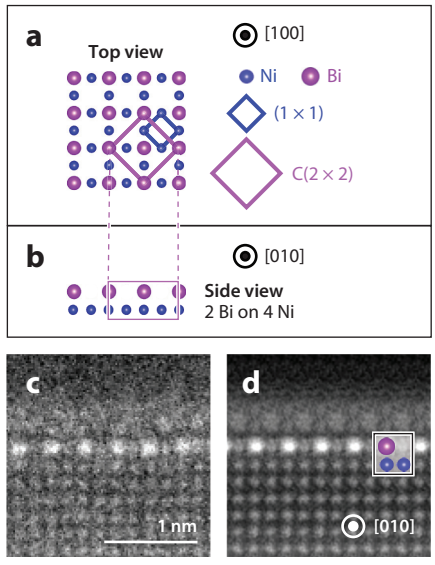

Figure 4

A Bi-rich grain boundary complexion in a Ni-Bi alloy. (*a*) Schematic top view and (*b*) side view of a Bi-rich adsorbate superstructure along the boundary predicted by density functional theory calculations. (*c*) High-angle annular dark-field–scanning transmission electron microscopy (HAADF-STEM) image of the grain boundary. (*d*) Filtered HAADF-STEM image, which more clearly reveals atomic positions. Atomic periodicity is seen only on one side of the grain boundary because it is a general, nonsymmetric boundary. Figure adapted with permission from Reference 84.

direction [010]. DFT calculations were then employed to predict adsorbate structures along the grain boundary plane, and these computationally predicted superstructures were remarkably consistent with the HAADF-STEM images when viewed in projection. This study highlights the benefit of combining computation with experiment when studying grain boundary complexions.

In addition, S/TEM imaging of a complexion can be affected by beam misalignment with the boundary plane as well as overlapping grains in the beam direction. Finally, chemical information is averaged over the thickness of the sample, again with a loss of three-dimensional information. APT offers yet another method for quantifying local composition, with an automated approach recently presented by Peng et al. (93). While APT lacks the atomic resolution required to measure complexion structure, it can be spatially correlated with TEM measurements from a common sample to overcome this limitation (94). We note that TEM and APT methods are both relatively low-throughput methods and are therefore limited to studying relatively small numbers of boundaries rather than analyzing the full distribution of grain boundary complexions in the system.

6. MODELING AND COMPUTATIONAL TOOLS

Computational methods provide valuable insight into grain boundary complexion behavior that is obscured by experimental and characterization limitations. Simple models that describe grain boundary complexions and their transitions are inspired by models for bulk alloys (e.g., lattice gas) and physisorption on free surfaces. For example, De Oliveira & Griffiths (95) and Pandit et al. (96) used a lattice-gas model to describe first-order layering transitions of gas adsorption on a homogeneous substrate. Although these models provide a useful starting point, they do not account for

variations in grain boundary geometry that significantly complicate the realistic modeling of grain boundary complexions and transitions.

A lattice-gas model of a grain boundary can be formulated by incorporating the interaction between segregating atoms and the boundary. To a first approximation, oversized atoms will move preferentially to the boundary to reduce strain energy because the boundary is relatively open compared to the bulk. Wynblatt & Shi (97) developed a lattice-gas-based model that includes these elastic driving forces for segregation, and Wynblatt & Chatain (98) were perhaps the first to observe a complexion transition in a regular-solution-based model of a polycrystal. More recently, Rickman et al. (99) numerically investigated layering (i.e., complexion) transitions at grain boundaries in a lattice-gas model of a binary alloy. In addition, Luo (100) advanced a lattice-gas model of internal interfaces that exhibits prewetting and roughening transitions.

As a simple illustration of a lattice-gas description of complexion states, consider a grain boundary in a bicrystal comprised of a binary, elastically isotropic solid, with A and B atoms arranged in two simple cubic lattices (99, 101). For this system, the occupancy variable associated with each lattice site is equal to zero (one) if it is occupied by an A (B) atom. The energetics are described by an Ising-like Hamiltonian originally employed for gas adsorption and tailored for this system. The thermodynamics are described by the free energy Ω, for thermally averaged site occupancy variables at temperature T, with an interaction energy between a misfitting atom and the grain boundary V, and chemical potential difference $\Delta\mu$. The equilibrium state is obtained by finding the occupancy variables that minimize Ω. The resulting coupled, transcendental equations can be solved for the occupancy variables to determine the amount of boundary segregation, i.e., the grain boundary excess. The results can be summarized in the form of grain boundary complexion diagrams that reflect the equilibrium state of the boundary (99). The limiting case of a high-angle boundary is considered here. **Figure 5** shows the dependence of grain boundary excess on the

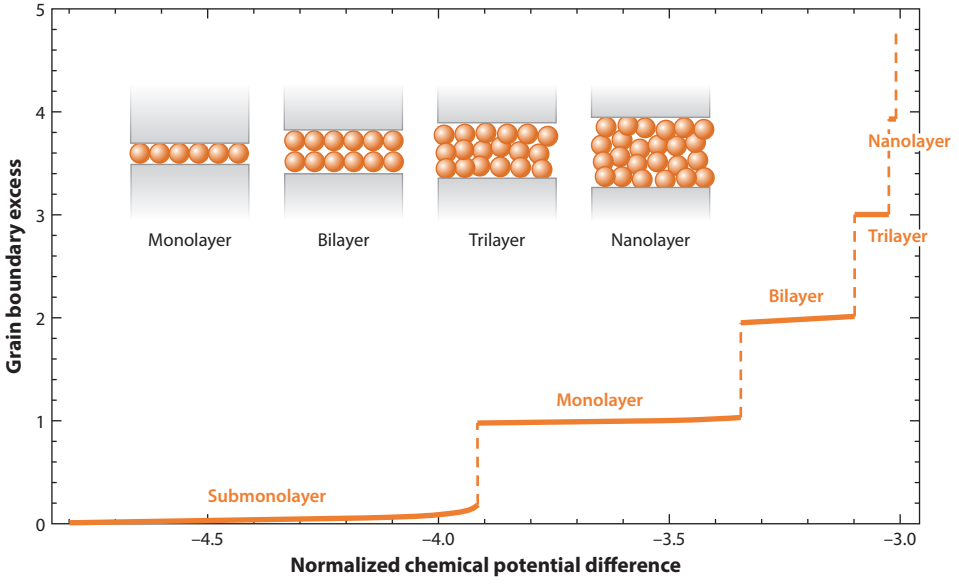

Figure 5

The dependence of the boundary excess on the normalized chemical potential difference, which is related to the bulk composition. Note the steps that indicate a series of sharp, first-order layering transitions. Figure adapted with permission from Reference 99.

normalized chemical potential difference, which is related to the bulk composition. The system exhibits a series of sharp, first-order layering complexion transitions, which are graphically illustrated in the inset schematic diagrams.

We now turn our attention to atomic-scale approaches, including MD and MC simulations. A common approach to constructing grain boundaries in atomistic simulations is the so-called gamma surface method (102), where the boundary is created by joining two misoriented crystals followed by a total energy minimization procedure. The procedure is repeated for different grain translations to find the lowest energy configuration. While this method can predict experimentally observed grain boundaries (102), early work demonstrated significant limitations that can result in incorrect predictions (103). The main limitations are that a relatively small number of possible grain boundary configurations are sampled, and no attempt is made to optimize the number of atoms at the boundary.

For example, twist boundaries in MgO (103) generated with the gamma surface method have relatively high energies and are nearly unstable with respect to spontaneously cleaving into surfaces. This prediction contradicts the experimental observation of stable twist boundaries (104). In 1983, Tasker & Duffy (103) showed that stable, low-energy structures of these grain boundaries can be obtained by removing a certain fraction of same-charge ions from the boundary. These simulations suggested that grain boundaries should be simulated in the grand-canonical ensemble where atoms can be inserted and removed to achieve equilibrium.

While the efficient grand-canonical simulation of solids remains an unsolved modeling challenge, some computational schemes have proven useful for identifying and modeling more realistic grain boundaries, which is a critical step toward modeling grain boundary complexion transitions more realistically. For example, simulated quenching to the zero-temperature limit of the grand-canonical ensemble of grain boundaries in fcc metals revealed new low-energy states with different atomic densities (105, 106). These simulations demonstrated that changes in grain boundary structure can be triggered by changing the chemical potential of the atoms. Optimizing the number of atoms at the boundary was also shown to be important for modeling realistic Si grain boundaries, for which the gamma surface approach predicted disordered or amorphous structures even at 0 K.

von Alfthan et al. (107) used a simulated annealing method to optimize grain boundary structures with different numbers of removed atoms and predicted new ordered, low-energy states. Chua et al. (108) also used genetic algorithms to perform grain boundary structure searches and explore possible configurations missed by the gamma surface method. The search predicted several ordered structures with different amounts of segregation. Grain boundary complexion diagrams for this system were proposed on the basis of the lowest free-energy criterion.

To allow the number of atoms at a grain boundary to vary, a new modeling approach was recently proposed (36). This approach uses high-temperature MD simulations with the boundaries connected to an open surface serving as a source/sink of atoms that allows density variations, thereby making complexion transitions possible. First-order structural complexion transitions and new ground state structures were found with this approach in two high-angle, high-energy (001)-symmetric tilt grain boundaries in Cu, Ag, Au, and Ni (36). This improved methodology demonstrated fully reversible, first-order transitions between complexions.

The discovery of new ground state structures and first-order grain boundary complexion transitions, as discussed above, suggests that conventional MD and MC methodologies that use periodic boundary conditions and constant numbers of atoms are insufficient to predict some complexion transitions. To improve the modeling of complexion transitions, the grain boundary structure must be grand-canonically optimized. For finite temperature simulations, this requires advanced structure sampling techniques and grand-canonical simulations of solids. Such techniques are yet

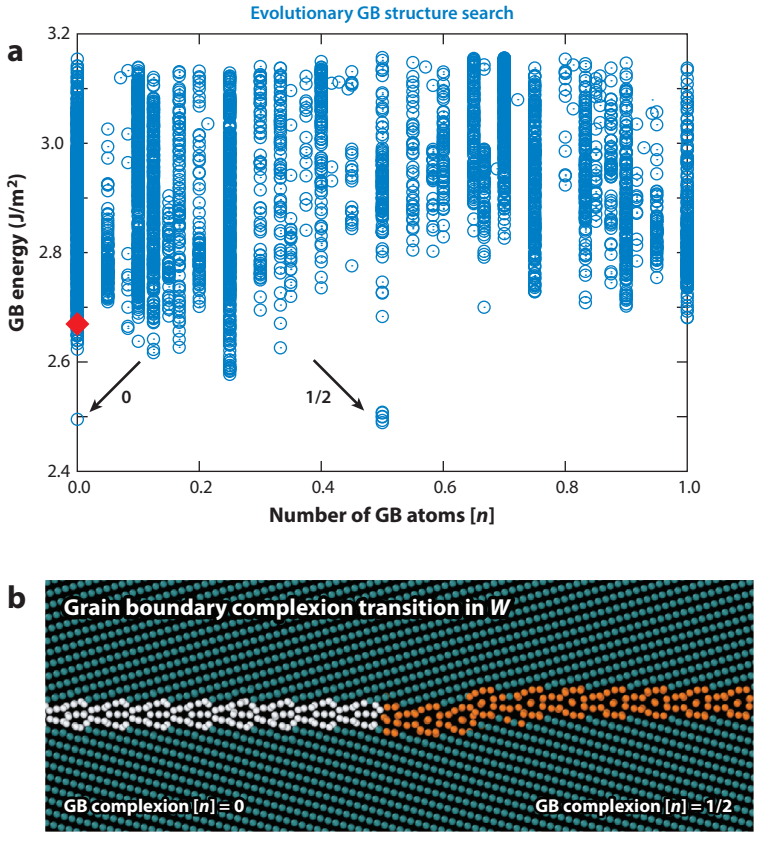

Figure 6

(*a*) Evolutionary grain boundary (GB) structure search performed with code USPEX for a high-angle, high-energy (109) symmetric tilt GB in tungsten. Blue circles correspond to the different GB structures generated by the algorithm. GB energy is plotted as a function of number of atoms [*n*]. The search outperforms the simple gamma surface construction (*red diamond*) and predicts two different GB complexions with different numbers of atoms [*n*] = 0 and [*n*] = 1/2. (*b*) Two GB complexions predicted by USPEX search at 0 K coexist at finite temperature, confirming that they are indeed examples of GB complexions. Figure adapted from Reference 56 with permission from The Royal Society of Chemistry.

to be developed. However, crystal structure prediction methods have been used to efficiently explore grain boundary structure and discover different complexions at 0 K (55).

USPEX is a leading computational tool that uses evolutionary algorithms to predict structures of crystals based on composition (109). Recently, Zhu et al. (55) extended this tool to grain boundary structure prediction. The algorithm generates a population of different grain boundary structures and improves them over several generations by operations of heredity and mutations to find the lowest energy configuration. This search explores a variety of structures, inserts and removes atoms to optimize atomic density, and replicates the boundary cross section to find larger area reconstructions.

A typical result of such a search is illustrated in **Figure 6*a***, with the energy of generated structures plotted as a function of the number of atoms, [*n*]. For comparison, the lowest energy structure generated by the gamma surface approach is shown. It is located at [*n*] = 0 since no atoms were inserted or removed. The evolutionary search outperforms the simple gamma

surface construction and finds structures with much lower energy. Note that although the new ground state at $[n] = 1/2$ requires that half of a plane of atoms be inserted, another minimum at $[n] = 0$ shows that a lower energy configuration can be obtained with the same number of atoms by simply rearranging them. The two new minima at $[n] = 0$ and $[n] = 1/2$ represent two different grain boundary complexions that can coexist at finite temperature, as shown in **Figure 6*b***. The evolutionary search with USPEX was also used to perform grain boundary structure searches for several different bcc metals, including W, Ta, and Mo, and different types of boundaries (56). New ground states, multiple complexions, and structural transformations at high temperature were observed in both high- and low-angle grain boundaries (110). More recently, Banadaki et al. (34) proposed a Monte Carlo sampling scheme that allows for efficient insertion and removal of atoms to optimize grain boundary structure at 0 K, and Gao et al. (111) used particle swarm optimization algorithms to perform grain boundary structure searches in multicomponent ceramics.

7. EQUILIBRIUM AND KINETIC COMPLEXION DIAGRAMS

Analogous to bulk phase diagrams, equilibrium complexion diagrams can be constructed with respect to temperature, pressure, and composition. However, complexions also depend on grain boundary geometry. Therefore, a polycrystal may have thousands of complexions, each with its own diagram. During grain growth, however, the system reconfigures to lower energy states, causing certain low-energy geometries to be overrepresented in the microstructure (77). Therefore, the system may well be described by a single average complexion diagram. Such diagrams can be useful, especially if the complexions in question dominate the material's behavior. For example, Zhou & Luo (112) used transition bands rather than transition lines and assumed that the grain boundary energy would vary ±15% to account for anisotropy.

Complexion diagrams have been constructed for many material systems, including binary and multicomponent metallic alloys (66, 101, 113–116) and doped ceramics (1, 64). An example of a complexion diagram overlaid on a bulk phase diagram is presented in **Figure 7*a***. This diagram is

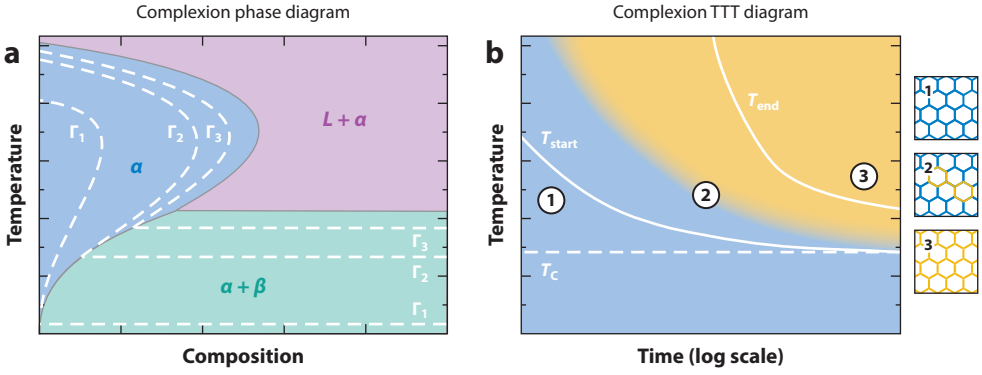

Figure 7

(*a*) A representative complexion diagram overlaid on a bulk phase diagram, based on the Mo-Ni complexion diagram in Reference 116. Complexion transition temperatures (*white dashed lines*) are labeled with the thickness (Γ_n) of the complexion type. (*b*) A schematic of a complexion time-temperature-transformation (TTT) diagram based on the experimentally derived diagram for Eu-doped $MgAl_2O_4$ in Reference 117. The insets depict the fraction of grain boundaries transformed to the high-temperature complexion type (*yellow grain boundaries*) at three different times marked in the diagram. T_C, T_{start}, and T_{end} are the complexion transition temperature, start time, and end time curves, respectively. Panel *a* adapted with permission from Reference 116, and panel *b* adapted with permission from Reference 117.

based on the Mo-Ni system (116) in which complexion transitions were identified by combining thermodynamic calculations with sintering experiments. The complexion transition lines, labeled with complexion thickness (Γ_n), show that the transition temperature changes with composition. Overlaying the complexion diagram on the bulk phase diagram provides insight into the relationship between bulk phase and grain boundary complexion behavior.

The exact mechanism by which grain boundary complexion transitions occur has not yet been definitively determined, although behavior suggestive of the kinetic nucleation and growth of complexion transitions has been observed in previous studies (73, 117, 118), where the fraction of boundaries transformed increases over time. Similarly, theoretical studies have suggested that complexion transitions are first-order transitions (99). However, experiments to interrogate the kinetics of complexion transitions are hindered by the lack of direct, in situ measurements. Thus, only a few kinetic diagrams, i.e., complexion time-temperature-transformation (TTT) diagrams, have been constructed. Although few in number, these complexion TTT diagrams represent a major conceptual advance with the potential to lead to new approaches in materials processing.

Unlike bulk phase TTT diagrams, which provide the time and temperature for a bulk phase to nucleate and grow, complexion TTT diagrams provide the time and temperature at which enough grain boundaries have transitioned to cause a noteworthy change in macroscopic behavior. While they do not directly indicate the nucleation and growth of a single complexion, they provide useful information for processing materials. **Figure 7*b*** shows an example TTT diagram based on the diagram for Eu-doped $MgAl_2O_4$ (117). It depicts a simple system with one dominant complexion at high and low temperatures with a transition temperature, T_C. In this system, the complexion transitions result in abnormal grain growth. The T_{start} line in **Figure 7*b*** indicates the time at each temperature where the abnormal grain growth begins after a sufficient number of complexion transitions, while the T_{end} line indicates that the majority of the grain boundaries have transitioned to the high-temperature complexion such that the microstructure contains only large grains. This diagram therefore provides a processing tool that guides users on the temperatures and times needed during annealing to achieve a specific microstructure.

However, since each unique grain boundary may have its own TTT diagram, highly anisotropic systems may require multiple complexion TTT diagrams for better prediction of properties, as done with Al_2O_3 (118). Despite such challenges, these diagrams form the basis of complexion engineering by providing a tool for predicting the behavior of polycrystals and for tailoring microstructures for better property control.

8. GRAIN BOUNDARY COMPLEXION ENGINEERING

Grain boundary complexion engineering can be employed to achieve desired macroscopic properties by tailoring grain boundary properties for a variety of applications. For example, abnormal grain growth with grain shape anisotropy can enhance fracture resistance via crack deflection (119), and this grain shape anisotropy can be controlled by inducing complexion transitions to create a subset of grain boundaries with high velocity. Conversely, selective doping can limit abnormal grain growth in materials when it is undesirable, such as in commercial-grade alumina (120). Nanocrystalline metals and ceramics can be thermally stabilized against grain growth if a slow velocity complexion, with a low grain boundary energy, is intentionally trapped within the microstructure (121). Solid-state, single-crystal conversion, where a single grain with high-velocity boundaries consumes the entire microstructure, is also possible using complexion engineering (122).

Nanolayer films, which are sometimes referred to as intergranular films, are commonly employed to improve mechanical and transport properties. For example, Zr-enriched nanolayer films

in nanocrystalline Cu-Zr alloys improve both strength and toughness by absorbing dislocations during plastic deformation (66). A similar approach is used to toughen ultrahard armor ceramics, namely, boron carbide and boron suboxide, against ballistic impacts. In this case, relatively weak nanolayers composed of various oxide additives promote intergranular fracture and enable crack deflection (123, 124). In addition to improving mechanical properties, nanolayer films can accelerate the densification of ceramics and metals by activated sintering (64). Recent results also suggest that, under certain conditions, flash sintering may also be initiated by grain boundary complexion transitions (125). Complexions can also reduce grain boundary diffusivity to resist high-temperature oxidation (126, 127) and creep (128, 129). For example, adding CuO to TiO_2 stabilizes a nanolayer complexion that enables activated sintering of powders 300°C below the eutectic temperature via enhanced grain boundary diffusivity (64). In $MgAl_2O_4$, different dopants (Eu and Yb) create similar monolayer-type complexions that exhibit dramatically different fracture resistance (70, 130).

Ionic, electrical, and thermal conductivity can also be controlled via complexion engineering. For example, ionic conductivity in electroceramics can be enhanced by over two orders of magnitude by tailoring the solute concentration to influence the complexion behavior (131). Electrically conductive or insulative complexions can be developed to modify bulk electrical conductivity, e.g., by Cu-rich oxide doping of alumina (89) and by the presence of Mg deficiencies near grain boundaries in Mg_3Sb_2 thermoelectric materials (132). Finally, specific grain boundary complexions in Skutterudite materials have been shown to reduce thermal conductivity by a factor of three to five (133).

9. FUTURE CHALLENGES

There has been much progress in the study of grain boundary complexion transitions in recent years. However, many challenges remain. Some of the most important challenges include the development of the following:

- Methods to directly identify grain boundary complexion transitions in situ in polycrystalline materials, rather than using indirect markers such as abnormal grain growth;
- Approaches to quantify the kinetics of complexion nucleation and growth; the above mentioned in situ methods may be useful in this pursuit;
- New complexion diagrams for both model material systems and engineering materials, including equilibrium and TTT complexion diagrams;
- Efficient approaches to the grand-canonical optimization of grain boundary structures to serve as the foundation of realistic grain boundary complexion simulations;
- The infusion of grain boundary engineering (134, 135) and grain boundary segregation engineering (136) with the knowledge gained in complexion studies to create a holistic approach to grain boundary complexion engineering (13).

10. CONCLUSION

Grain boundary complexion transitions can result in discontinuous changes in grain boundary properties and, accordingly, rapid and sometimes anomalous changes in the properties of polycrystalline materials. These transitions can occur under conditions distinct from bulk phase transformations where such changes are typically unexpected. As noted above, these changes may sometimes be detrimental but, in many cases, can be enormously beneficial. Grain boundary complexion engineering (13) offers the promise of improving the processing, properties, and performance of

materials by carefully controlling complexion transitions. Future work should support the development of grain boundary complexion diagrams, which will provide the necessary guidance to enable complexion engineering to be more widely employed by the general materials science and engineering community.

DISCLOSURE STATEMENT

The authors are not aware of any affiliations, memberships, funding, or financial holdings that might be perceived as affecting the objectivity of this review.

ACKNOWLEDGMENTS

P.R.C. gratefully acknowledges support from the Rose-Hulman Institute of Technology Summer Professional Development Grants program. Support for T.F. was provided under the auspices of the US Department of Energy by Lawrence Livermore National Laboratory (LLNL) under Contract DE-AC52-07NA27344. T.F. was funded by the Laboratory Directed Research and Development Program at LLNL under Project Tracking Code 19-ERD-026. T.J.R. gratefully acknowledges support from the US Army Research Office under grant W911NF-16-1-0369 and the US Department of Energy, Office of Basic Energy Sciences, Materials Science and Engineering Division under award DE-SC0014232. C.J.M., J.M.R., and M.P.H. gratefully acknowledge the financial support of the Army Research Office under contract W911NF-19-2-0093, program manager Michael P. Bakas.

LITERATURE CITED

1. Cantwell PR, Tang M, Dillon SJ, Luo J, Rohrer GS, Harmer MP. 2014. Grain boundary complexions. *Acta Mater.* 62:1–48
2. Tang M, Carter WC, Cannon RM. 2006. Diffuse interface model for structural transitions of grain boundaries. *Phys. Rev. B* 73(2):024102
3. Harmer MP. 2011. The phase behavior of interfaces. *Science* 332(6026):182–83
4. Dillon SJ, Tai K, Chen S. 2016. The importance of grain boundary complexions in affecting physical properties of polycrystals. *Curr. Opin. Solid State Mater. Sci.* 20(5):324–35
5. Gupta VK, Yoon D-H, Meyer HM, Luo J. 2007. Thin intergranular films and solid-state activated sintering in nickel-doped tungsten. *Acta Mater.* 55(9):3131–42
6. Luo J, Cheng H, Asl KM, Kiely CJ, Harmer MP. 2011. The role of a bilayer interfacial phase on liquid metal embrittlement. *Science* 333(6050):1730–33
7. Dillon SJ, Tang M, Carter WC, Harmer MP. 2007. Complexion: a new concept for kinetic engineering in materials science. *Acta Mater.* 55(18):6208–18
8. Hart EW. 1968. Two-dimensional phase transformation in grain boundaries. *Scr. Metall.* 2(3):179–82
9. Hart EW. 1972. Grain boundary phase transformations. In *The Nature and Behavior of Grain Boundaries*, ed. H Hu, pp. 155–70. New York: Plenum Press
10. Cahn JW. 1982. Transitions and phase equilibria among grain boundary structures. *J. Phys. Colloq.* 43:C6-199–213
11. Tang M, Carter WC, Cannon RM. 2006. Grain boundary transitions in binary alloys. *Phys. Rev. Lett.* 97(7):075502
12. Clarke DR, Thomas G. 1977. Grain boundary phases in a hot-pressed MgO fluxed silicon nitride. *J. Am. Ceram. Soc.* 60(11–12):491–95
13. Krause AR, Cantwell PR, Marvel CJ, Compson C, Rickman JM, Harmer MP. 2019. Review of grain boundary complexion engineering: know your boundaries. *J. Am. Ceram. Soc.* 102(2):778–800

14. Wynblatt P, Chatain D. 2006. Anisotropy of segregation at grain boundaries and surfaces. *Metall. Mater. Trans. A* 37(9):2595–620
15. Günter G, Shvindlerman LS. 2009. *Grain Boundary Migration in Metals: Thermodynamics, Kinetics, Applications*. Boca Raton, FL: CRC Press. 2nd ed.
16. Herring C. 1951. Surface tension as a motivation for sintering. In *The Physics of Powder Metallurgy*, ed. WE Kingston, pp. 143–79. New York: McGraw-Hill
17. Gibbs JW. 1948. *The Collected Works of J.W. Gibbs*, Vol. 1. New Haven, CT: Yale Univ. Press
18. Cahn JW. 1977. Thermodynamics of solid and fluid interfaces. In *Interfacial Segregation: Papers Presented at a Seminar of the Materials Science Division of the American Society for Metals, October 22 and 23, 1977*, ed. WC Johnson, JM Blakely, pp. 3–23. Metals Park, OH: Am. Soc. Met.
19. Frolov T, Mishin Y. 2015. Phases, phase equilibria, and phase rules in low-dimensional systems. *J. Chem. Phys.* 143(4):044706
20. Rohrer GS. 2016. The role of grain boundary energy in grain boundary complexion transitions. *Curr. Opin. Solid State Mater. Sci.* 20(5):231–39
21. Frolov T, Mishin Y. 2012. Thermodynamics of coherent interfaces under mechanical stresses. I. Theory. *Phys. Rev. B* 85(22):224106
22. Rottman C. 1988. Theory of phase transitions at internal interfaces. *J. Phys. Colloq.* 49:C5-313–26
23. Sigle W, Ciiang L-S, Gusr W. 2002. On the correlation between grain-boundary segregation, faceting and embrittlement in Bi-doped Cu. *Philos. Mag. A* 82(8):1595–608
24. Kundu A, Asl KM, Luo J, Harmer MP. 2013. Identification of a bilayer grain boundary complexion in Bi-doped Cu. *Scr. Mater.* 68(2):146–49
25. Mullins WW. 1957. Theory of thermal grooving. *J. Appl. Phys.* 28(3):333–39
26. Saylor DM, Rohrer GS. 1999. Measuring the influence of grain-boundary misorientation on thermal groove geometry in ceramic polycrystals. *J. Am. Ceram. Soc.* 82(6):1529–36
27. Dillon SJ, Harmer MP, Rohrer GS. 2010. The relative energies of normally and abnormally growing grain boundaries in alumina displaying different complexions. *J. Am. Ceram. Soc.* 93(6):1796–802
28. Bojarski SA, Ma S, Lenthe W, Harmer MP, Rohrer GS. 2012. Changes in the grain boundary character and energy distributions resulting from a complexion transition in Ca-doped yttria. *Metall. Mater. Trans. A* 43(10):3532–38
29. Quach DV, Castro RHR. 2012. Direct measurement of grain boundary enthalpy of cubic yttria-stabilized zirconia by differential scanning calorimetry. *J. Appl. Phys.* 112(8):083527
30. Muche DNF, Marple MAT, Sen S, Castro RHR. 2018. Grain boundary energy, disordering energy and grain growth kinetics in nanocrystalline $MgAl_2O_4$ spinel. *Acta Mater.* 149:302–11
31. Dey S, Chang C-H, Gong M, Liu F, Castro RHR. 2015. Grain growth resistant nanocrystalline zirconia by targeting zero grain boundary energies. *J. Mater. Res.* 30(20):2991–3002
32. Cheng J, Luo J, Yang K. 2018. Aimsgb: an algorithm and open-source python library to generate periodic grain boundary structures. *Comput. Mater. Sci.* 155:92–103
33. Tschopp MA, Coleman SP, McDowell DL. 2015. Symmetric and asymmetric tilt grain boundary structure and energy in Cu and Al (and transferability to other fcc metals). *Integr. Mater. Manuf. Innov.* 4(1):176–89
34. Banadaki AD, Tschopp MA, Patala S. 2018. An efficient Monte Carlo algorithm for determining the minimum energy structures of metallic grain boundaries. *Comput. Mater. Sci.* 155:466–75
35. Olmsted DL, Buta D, Adland A, Foiles SM, Asta M, Karma A. 2011. Dislocation-pairing transitions in hot grain boundaries. *Phys. Rev. Lett.* 106(4):046101
36. Frolov T, Olmsted DL, Asta M, Mishin Y. 2013. Structural phase transformations in metallic grain boundaries. *Nat. Commun.* 4:1899
37. Frolov T, Asta M, Mishin Y. 2015. Segregation-induced phase transformations in grain boundaries. *Phys. Rev. B* 92(2):020103
38. Brown JA, Mishin Y. 2007. Dissociation and faceting of asymmetrical tilt grain boundaries: molecular dynamics simulations of copper. *Phys. Rev. B* 76(13):134118
39. Rickman JM, Harmer MP, Chan HM. 2016. Grain-boundary layering transitions and phonon engineering. *Surf. Sci.* 651:1–4

40. Hickman J, Mishin Y. 2016. Disjoining potential and grain boundary premelting in binary alloys. *Phys. Rev. B* 93(22):224108
41. Merkle KL, Smith DJ. 1987. Atomic structure of symmetric tilt grain boundaries in NiO. *Phys. Rev. Lett.* 59(25):2887–90
42. Sickafus KE, Sass SL. 1987. Grain boundary structural transformations induced by solute segregation. *Acta Metall.* 35(1):69–79
43. Khalajhedayati A, Rupert TJ. 2015. High-temperature stability and grain boundary complexion formation in a nanocrystalline Cu-Zr alloy. *JOM* 67(12):2788–801
44. Luo J, Shi X. 2008. Grain boundary disordering in binary alloys. *Appl. Phys. Lett.* 92(10):101901
45. Ma S, Asl KM, Tansarawiput C, Cantwell PR, Qi M, et al. 2012. A grain boundary phase transition in Si-Au. *Scr. Mater.* 66(5):203–6
46. Ma S, Cantwell PR, Pennycook TJ, Zhou N, Oxley MP, et al. 2013. Grain boundary complexion transitions in WO_3- and CuO-doped TiO_2 bicrystals. *Acta Mater.* 61(5):1691–704
47. Peter NJ, Frolov T, Duarte MJ, Hadian R, Ophus C, et al. 2018. Segregation-induced nanofaceting transition at an asymmetric tilt grain boundary in copper. *Phys. Rev. Lett.* 121(25):255502
48. Kwiatkowski da Silva A, Ponge D, Peng Z, Inden G, Lu Y, et al. 2018. Phase nucleation through confined spinodal fluctuations at crystal defects evidenced in Fe-Mn alloys. *Nat. Commun.* 9(1):1137
49. Zhou X, Yu X, Kaub T, Martens RL, Thompson GB. 2016. Grain boundary specific segregation in nanocrystalline Fe(Cr). *Sci. Rep.* 6:34642
50. Williams PL, Mishin Y. 2009. Thermodynamics of grain boundary premelting in alloys. II. Atomistic simulation. *Acta Mater.* 57(13):3786–94
51. Pan Z, Rupert TJ. 2016. Effect of grain boundary character on segregation-induced structural transitions. *Phys. Rev. B* 93(13):134113
52. O'Brien CJ, Barr CM, Price PM, Hattar K, Foiles SM. 2018. Grain boundary phase transformations in PtAu and relevance to thermal stabilization of bulk nanocrystalline metals. *J. Mater. Sci.* 53(4):2911–27
53. Yang S, Zhou N, Zheng H, Ong SP, Luo J. 2018. First-order interfacial transformations with a critical point: breaking the symmetry at a symmetric tilt grain boundary. *Phys. Rev. Lett.* 120(8):085702
54. Pan Z, Rupert TJ. 2017. Spatial variation of short-range order in amorphous intergranular complexions. *Comput. Mater. Sci.* 131:62–68
55. Zhu Q, Samanta A, Li B, Rudd RE, Frolov T. 2018. Predicting phase behavior of grain boundaries with evolutionary search and machine learning. *Nat. Commun.* 9(1):467
56. Frolov T, Setyawan W, Kurtz RJ, Marian J, Oganov AR, et al. 2018. Grain boundary phases in bcc metals. *Nanoscale* 10(17):8253–68
57. Tewari A, Nabiei F, Cantoni M, Bowen P, Hébert C. 2014. Segregation of anion (Cl^-) impurities at transparent polycrystalline α-alumina interfaces. *J. Eur. Ceram. Soc.* 34(12):3037–45
58. Molodov DA, Czubayko U, Gottstein G, Shvindlerman LS, Straumal B, Gust W. 1995. Acceleration of grain boundary motion in Al by small additions of Ga. *Philos. Mag. Lett.* 72(6):361–68
59. Dillon SJ, Harmer MP. 2007. Multiple grain boundary transitions in ceramics: a case study of alumina. *Acta Mater.* 55(15):5247–54
60. Divinski S, Lohmann M, Herzig C, Straumal B, Baretzky B, Gust W. 2005. Grain-boundary melting phase transition in the Cu-Bi system. *Phys. Rev. B* 71(10):104104
61. Divinski SV, Edelhoff H, Prokofjev S. 2012. Diffusion and segregation of silver in copper Σ5(310) grain boundary. *Phys. Rev. B* 85(14):144104
62. Frolov T, Divinski SV, Asta M, Mishin Y. 2013. Effect of interface phase transformations on diffusion and segregation in high-angle grain boundaries. *Phys. Rev. Lett.* 110(25):255502
63. Prokoshkina D, Esin VA, Divinski SV. 2017. Experimental evidence for anomalous grain boundary diffusion of Fe in Cu and Cu-Fe alloys. *Acta Mater.* 133:240–46
64. Nie J, Chan JM, Qin M, Zhou N, Luo J. 2017. Liquid-like grain boundary complexion and sub-eutectic activated sintering in CuO-doped TiO_2. *Acta Mater.* 130:329–38
65. Sigle W, Richter G, Rühle M, Schmidt S. 2006. Insight into the atomic-scale mechanism of liquid metal embrittlement. *Appl. Phys. Lett.* 89(12):121911

66. Khalajhedayati A, Pan Z, Rupert TJ. 2016. Manipulating the interfacial structure of nanomaterials to achieve a unique combination of strength and ductility. *Nat. Commun.* 7:10802
67. Pan Z, Rupert TJ. 2015. Amorphous intergranular films as toughening structural features. *Acta Mater.* 89:205–14
68. Turlo V, Rupert TJ. 2018. Grain boundary complexions and the strength of nanocrystalline metals: dislocation emission and propagation. *Acta Mater.* 151:100–11
69. Madhav Reddy K, Guo JJ, Shinoda Y, Fujita T, Hirata A, et al. 2012. Enhanced mechanical properties of nanocrystalline boron carbide by nanoporosity and interface phases. *Nat. Commun.* 3:1052
70. Cui FY, Kundu A, Krause A, Harmer MP, Vinci RP. 2018. Surface energies, segregation, and fracture behavior of magnesium aluminate spinel low-index grain boundary planes. *Acta Mater.* 148:320–29
71. Feng L, Hao R, Lambros J, Dillon SJ. 2018. The influence of dopants and complexion transitions on grain boundary fracture in alumina. *Acta Mater.* 142:121–30
72. Rohrer GS. 2011. Grain boundary energy anisotropy: a review. *J. Mater. Sci.* 46(18):5881–95
73. Bojarski SA, Harmer MP, Rohrer GS. 2014. Influence of grain boundary energy on the nucleation of complexion transitions. *Scr. Mater.* 88:1–4
74. Li J, Dillon SJ, Rohrer GS. 2009. Relative grain boundary area and energy distributions in nickel. *Acta Mater.* 57(14):4304–11
75. Ratanaphan S, Olmsted DL, Bulatov VV, Holm EA, Rollett AD, Rohrer GS. 2015. Grain boundary energies in body-centered cubic metals. *Acta Mater.* 88:346–54
76. Olmsted DL, Foiles SM, Holm EA. 2009. Survey of computed grain boundary properties in face-centered cubic metals: I. Grain boundary energy. *Acta Mater.* 57(13):3694–703
77. Dillon SJ, Rohrer GS. 2009. Mechanism for the development of anisotropic grain boundary character distributions during normal grain growth. *Acta Mater.* 57(1):1–7
78. Kelly MN, Bojarski SA, Rohrer GS. 2017. The temperature dependence of the relative grain-boundary energy of yttria-doped alumina. *J. Am. Ceram. Soc.* 100(2):783–91
79. Dillon SJ, Harmer MP, Rohrer GS. 2010. Influence of interface energies on solute partitioning mechanisms in doped aluminas. *Acta Mater.* 58(15):5097–108
80. Rheinheimer W, Hoffmann MJ. 2015. Non-Arrhenius behavior of grain growth in strontium titanate: new evidence for a structural transition of grain boundaries. *Scr. Mater.* 101:68–71
81. Sternlicht H, Rheinheimer W, Hoffmann MJ, Kaplan WD. 2016. The mechanism of grain boundary motion in $SrTiO_3$. *J. Mater. Sci.* 51(1):467–75
82. Kelly MN, Rheinheimer W, Hoffmann MJ, Rohrer GS. 2018. Anti-thermal grain growth in $SrTiO_3$: coupled reduction of the grain boundary energy and grain growth rate constant. *Acta Mater.* 149:11–18
83. Frazier WE, Rohrer GS, Rollett AD. 2015. Abnormal grain growth in the Potts model incorporating grain boundary complexion transitions that increase the mobility of individual boundaries. *Acta Mater.* 96:390–98
84. Yu Z, Cantwell PR, Gao Q, Yin D, Zhang Y, et al. 2017. Segregation-induced ordered superstructures at general grain boundaries in a nickel-bismuth alloy. *Science* 358(6359):97–101
85. Alber U, Mullejans H, Ruhle M. 1997. Improved quantification of grain boundary segregation by EDS in a dedicated STEM. *Ultramicroscopy* 69:105–16
86. Marvel CJ, Behler KD, LaSalvia JC, Domnich V, Haber RA, et al. 2019. Extending ζ-factor microanalysis to boron-rich ceramics: quantification of bulk stoichiometry and grain boundary composition. *Ultramicroscopy* 202:163–72
87. Sternlicht H, Bojarski SA, Rohrer GS, Kaplan WD. 2018. Quantitative differences in the Y grain boundary excess at boundaries delimiting large and small grains in Y doped Al_2O_3. *J. Eur. Ceram. Soc.* 38(4):1829–35
88. Liu C, Chen H, Nie JF. 2016. Interphase boundary segregation of Zn in Mg-Sn-Zn alloys. *Scr. Mater.* 123:5–8
89. Marvel CJ, Kracum MR, Yu Z, Harmer MP, Chan HM. 2018. Observation of Cu-rich grain boundary nanoparticles and complexions in Cu/Ti-doped alumina. *Scr. Mater.* 157:34–38
90. Herbig M, Raabe D, Li YJ, Choi P, Zaefferer S, Goto S. 2014. Atomic-scale quantification of grain boundary segregation in nanocrystalline material. *Phys. Rev. Lett.* 112(12):126103

91. Marvel CJ, Hornbuckle BC, Darling KA, Harmer MP. 2019. Intentional and unintentional elemental segregation to grain boundaries in a Ni-rich nanocrystalline alloy. *J. Mater. Sci.* 54(4):3496–508
92. Nguyen TD, La Fontaine A, Yang L, Cairney JM, Zhang J, Young DJ. 2018. Atom probe study of impurity segregation at grain boundaries in chromia scales grown in CO_2 gas. *Corros. Sci.* 132:125–35
93. Peng Z, Lu Y, Hatzoglou C, Kwiatkowski da Silva A, Vurpillot F, et al. 2019. An automated computational approach for complete in-plane compositional interface analysis by atom probe tomography. *Microsc. Microanal.* 25(2):389–400
94. Herbig M. 2018. Spatially correlated electron microscopy and atom probe tomography: current possibilities and future perspectives. *Scr. Mater.* 148:98–105
95. De Oliveira MJ, Griffiths RB. 1978. Lattice-gas model of multiple layer adsorption. *Surf. Sci.* 71(3):687–94
96. Pandit R, Schick M, Wortis M. 1982. Systematics of multilayer adsorption phenomena on attractive substrates. *Phys. Rev. B* 26(9):5112–40
97. Wynblatt P, Shi Z. 2005. Relation between grain boundary segregation and grain boundary character in FCC alloys. *J. Mater. Sci.* 40(11):2765–73
98. Wynblatt P, Chatain D. 2008. Solid-state wetting transitions at grain boundaries. *Mater. Sci. Eng. A* 495(1–2):119–25
99. Rickman JM, Chan HM, Harmer MP, Luo J. 2013. Grain-boundary layering transitions in a model bicrystal. *Surf. Sci.* 618:88–93
100. Luo J. 2009. Grain boundary complexions: the interplay of premelting, prewetting, and multilayer adsorption. *Appl. Phys. Lett.* 95(7):071911
101. Rickman JM, Luo J. 2016. Layering transitions at grain boundaries. *Curr. Opin. Solid State Mater. Sci.* 20(5):225–30
102. Sutton AP, Balluffi RW. 1995. *Interfaces in Crystalline Materials*. Oxford, UK: Clarendon Press
103. Tasker PW, Duffy DM. 1983. On the structure of twist grain boundaries in ionic oxides. *Philos. Mag. A* 47(6):L45–48
104. Sun CP, Balluffi RW. 1982. Secondary grain boundary dislocations in [001]twist boundaries in MgO I. Intrinsic structures. *Philos. Mag. A* 46(1):49–62
105. Phillpot SR, Rickman JM. 1992. Simulated quenching to the zero-temperature limit of the grand-canonical ensemble. *J. Chem. Phys.* 97(4):2651–58
106. Phillpot SR. 1994. Simulation of solids at nonzero temperatures in the grand-canonical ensemble. *Phys. Rev. B* 49(11):7639–45
107. von Alfthan S, Haynes PD, Kaski K, Sutton AP. 2006. Are the structures of twist grain boundaries in silicon ordered at 0 K? *Phys. Rev. Lett.* 96(5):055505
108. Chua AL-S, Benedek NA, Chen L, Finnis MW, Sutton AP. 2010. A genetic algorithm for predicting the structures of interfaces in multicomponent systems. *Nat. Mater.* 9(5):418–22
109. Oganov AR, Glass CW. 2006. Crystal structure prediction using ab initio evolutionary techniques: principles and applications. *J. Chem. Phys.* 124(24):244704
110. Frolov T, Zhu Q, Oppelstrup T, Marian J, Rudd RE. 2018. Structures and transitions in bcc tungsten grain boundaries and their role in the absorption of point defects. *Acta Mater.* 159:123–34
111. Gao B, Gao P, Lu S, Lv J, Wang Y, Ma Y. 2019. Interface structure prediction via CALYPSO method. *Sci. Bull.* 64(5):301–9
112. Zhou N, Luo J. 2015. Developing grain boundary diagrams for multicomponent alloys. *Acta Mater.* 91:202–16
113. Zhou N, Hu T, Luo J. 2016. Grain boundary complexions in multicomponent alloys: challenges and opportunities. *Curr. Opin. Solid State Mater. Sci.* 20(5):268–77
114. Straumal B, Gust W, Molodov D. 1994. Tie lines of the grain boundary wetting phase transition in the Al-Sn system. *J. Phase Equilib.* 15(4):386–91
115. Zhou N, Yu Z, Zhang Y, Harmer MP, Luo J. 2017. Calculation and validation of a grain boundary complexion diagram for Bi-doped Ni. *Scr. Mater.* 130:165–69
116. Shi X, Luo J. 2011. Developing grain boundary diagrams as a materials science tool: a case study of nickel-doped molybdenum. *Phys. Rev. B* 84(1):014105

117. Schumacher O, Marvel CJ, Kelly MN, Cantwell PR, Vinci RP, et al. 2016. Complexion time-temperature-transformation (TTT) diagrams: opportunities and challenges. *Curr. Opin. Solid State Mater. Sci.* 20(5):316–23
118. Cantwell PR, Ma S, Bojarski S, Rohrer G, Harmer MP. 2016. Expanding time-temperature-transformation (TTT) diagrams to interfaces: a new approach for grain boundary engineering. *Acta Mater*. 106:78–86
119. Peillon FC, Thevenot F. 2002. Microstructural designing of silicon nitride related to toughness. *J. Eur. Ceram. Soc.* 22(3):271–78
120. Lawrence AK, Kundu A, Harmer MP, Compson C, Atria J, Spreij M. 2015. Influence of complexion transitions on microstructure evolution in specialty aluminas. *J. Am. Ceram. Soc.* 98(4):1347–55
121. Saber M. 2013. *Thermal stability of nanocrystalline alloys by solute additions and a thermodynamic modeling*. PhD Thesis, N.C. State Univ., Raleigh, NC
122. Dillon SJ, Harmer MP. 2007. Mechanism of "solid-state" single-crystal conversion in alumina. *J. Am. Ceram. Soc.* 90(3):993–95
123. Coleman SP, Hernandez-Rivera E, Behler KD, Synowczynski-Dunn J, Tschopp MA. 2016. Challenges of engineering grain boundaries in boron-based armor ceramics. *JOM* 68(6):1605–15
124. Behler KD, Marvel CJ, LaSalvia JC, Walck SD, Harmer MP. 2018. Observations of grain boundary chemistry variations in a boron carbide processed with oxide additives. *Scr. Mater.* 142:106–10
125. Zhang Y, Nie J, Luo J. 2019. Flash sintering activated by bulk phase and grain boundary complexion transformations. *Acta Mater*. 181:544–54
126. Yu Z, Wu Q, Rickman JM, Chan HM, Harmer MP. 2013. Atomic-resolution observation of Hf-doped alumina grain boundaries. *Scr. Mater.* 68(9):703–6
127. Wu Q, Chan HM, Rickman JM, Harmer MP. 2015. Effect of Hf^{4+} concentration on oxygen grain-boundary diffusion in alumina. *J. Am. Ceram. Soc.* 98(10):3346–51
128. Reddy KV, Pal S. 2018. Effect of grain boundary complexions on the deformation behavior of Ni bicrystal during bending creep. *J. Mol. Model.* 24(4):87
129. Reddy KV, Pal S. 2018. Influence of grain boundary complexion on deformation mechanism of high temperature bending creep process of Cu bicrystal. *Trans. Indian Inst. Met.* 71(7):1721–34
130. Cao W, Kundu A, Yu Z, Harmer MP, Vinci RP. 2013. Direct correlations between fracture toughness and grain boundary segregation behavior in ytterbium-doped magnesium aluminate spinel. *Scr. Mater.* 69(1):81–84
131. Bowman WJ, Kelly MN, Rohrer GS, Hernandez CA, Crozier PA. 2017. Enhanced ionic conductivity in electroceramics by nanoscale enrichment of grain boundaries with high solute concentration. *Nanoscale* 9(44):17293–302
132. Kuo JJ, Yu Y, Kang SD, Cojocaru-Mirédin O, Wuttig M, Snyder GJ. 2019. Mg deficiency in grain boundaries of n-type Mg_3Sb_2 identified by atom probe tomography. *Adv. Mater. Interfaces* 6(13):1900429
133. Zong PA, Hanus R, Dylla M, Tang Y, Liao J, et al. 2017. Skutterudite with graphene-modified grain-boundary complexion enhances zT enabling high-efficiency thermoelectric device. *Energy Environ. Sci.* 10(1):183–91
134. Watanabe T. 1984. An approach to grain boundary design of strong and ductile polycrystals. *Res. Mech.* 11(1):47–84
135. Watanabe T. 2011. Grain boundary engineering: historical perspective and future prospects. *J. Mater. Sci.* 46(12):4095–115
136. Raabe D, Herbig M, Sandlöbes S, Li Y, Tytko D, et al. 2014. Grain boundary segregation engineering in metallic alloys: a pathway to the design of interfaces. *Curr. Opin. Solid State Mater. Sci.* 18(4):253–61
137. Duscher G, Chisholm MF, Alber U, Rühle M. 2004. Bismuth-induced embrittlement of copper grain boundaries. *Nat. Mater.* 3(9):621–26